JACS
JOURNAL OF THE AMERICAN CHEMICAL SOCIETY
Article
pubs.acs.org/JACS

Surface Acidity as Descriptor of Catalytic Activity for Oxygen Evolution Reaction in Li-O_2 Battery

Jinzhen Zhu,[†,∥] Fan Wang,[‡,∥] Beizhou Wang,[†] Youwei Wang, Jianjun Liu,*[,†] Wenqing Zhang,*[,†,§] and Zhaoyin Wen*[,‡]

[†]State Key Laboratory of High Performance Ceramics and Superfine Microstructure, [‡]CAS Key laboratory of Materials for Energy Conversion, Shanghai institute of Ceramics, Chinese Academy of Sciences, 1295 Dingxi Road, Shanghai 200050, China

[§]Materilas Genome Institute, Shanghai University, 99 Shangda Road, Shanghai 200444, China

Supporting Information

ABSTRACT: Unraveling the descriptor of catalytic activity, which is related to physical properties of catalysts, is a major objective of catalysis research. In the present study, the first-principles calculations based on interfacial model were performed to study the oxygen evolution reaction mechanism of Li_2O_2 supported on active surfaces of transition-metal compounds (TMC: oxides, carbides, and nitrides). Our studies indicate that the O_2 evolution and Li^+ desorption energies show linear and volcano relationships with surface acidity of catalysts, respectively. Therefore, the charging voltage and desorption energies of Li^+ and O_2 over TMC could correlate with their corresponding surface acidity. It is found that certain materials with an appropriate surface acidity can achieve the high catalytic activity in reducing charging voltage and activation barrier of rate-determinant step. According to this correlation, CoO should have as active catalysis as Co_3O_4 in reducing charging overpotential, which is further confirmed by our comparative experimental studies. Co_3O_4, Mo_2C, TiC, and TiN are predicted to have a relatively high catalytic activity, which is consistent with the previous experiments. The present study enables the rational design of catalysts with greater activity for charging reactions of Li-O_2 battery.

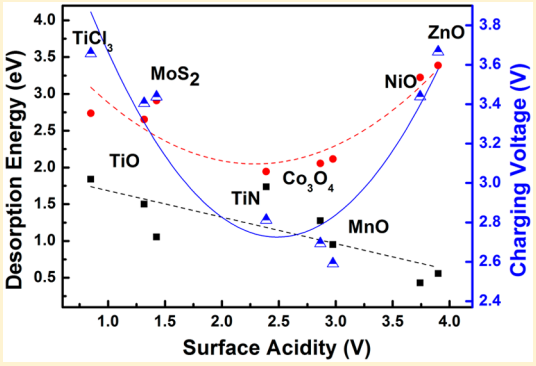

1. INTRODUCTION

There has been a tremendous interest in the field of catalysis to establish the descriptor of the catalytic activity and the selectivity correlated with physical properties of catalysts. An effective descriptor can be intensively applied to design a novel and highly active catalyst or structural optimization to improve catalytic activity for specific materials. For example, Hammer and Nørskov have developed a theoretical model of "d-band center" to describe the relationship of molecular adsorption strength on metal surface with the energy of the d-band center in the metal.[1] Such a model and extended models have proved useful to predict the catalytic activity of metal and alloys for many molecular reactions such as CO oxidation, O_2 reduction, and oxygen evolution reaction from water.[2−8] Inspired by the success of the d-band center model, many molecular reactions catalyzed by metal alloys and metal oxides were studied to identify the descriptors of catalytic activity.[2,5,9] However, extending the model of catalytic molecular reaction to catalytic reaction in solid−solid interface, developing an effective model to describe catalytic activity of solid−solid interfacial reaction, remains challenging due to complexity,[10] but highly desired for screening a novel catalyst.

Rechargeable lithium−oxygen batteries are considered as promising next-generation devices for energy storage and conversion because of their high theoretical specific energy (>3500 $Whkg^{-1}$), which is 3−5 times larger than that of current lithium-ion batteries.[10−16] However, they suffer from several issues such as high overpotential (0.5−1.2 V),[12,17,18] poor cycle performance,[18−20] and limited rate capability.[11,21,22] These critical challenges which limit its practical application are mainly ascribed to slightly slow oxygen reduction reaction (ORR: $2Li^+ + O_2 + 2e^- \rightarrow Li_2O_2$) and significantly sluggish oxygen evolution reaction (OER, $Li_2O_2 \rightarrow 2Li^+ + O_2 + 2e^-$). In the past several years, a great deal of research efforts were made to develop highly active catalysts to improve ORR and OER kinetics, such as transition-metal oxides (TMO),[8,9,15−20] noble metals,[14,23,24] carbonaceous materials, transition-metal carbide, and nitride, and perovskites.[25−27] Shao-Horn et al. performed systematic studies for some noble metals as ORR catalysts of Li-O_2 battery via rotating disk electrode measurements.[23] They established a volcano relationship of discharging voltages with oxygen adsorption energies. Later, Xu et al. performed extensive first-principles calculations for these catalytic mechanisms of noble metals and revealed consistent trend of catalytic activity.[28,29] The highest active catalyst should have an appropriate O adsorption strength close to those of well-established Pt and Pd catalysts.

Received: July 30, 2015
Published: October 5, 2015

DOI: 10.1021/jacs.5b07792
J. Am. Chem. Soc. 2015, 137, 13572−13579

In contrast, there are not many systematic experimental and theoretical studies to reveal underlying essence of catalytic activity for OER in Li-O_2 battery, although OER catalysts are more efficient than ORR catalysts in reducing charging−discharging overpotential and a large number of OER catalysts have been explored independently. However, identifying activity descriptors of OER in electrocatalytic water splitting has been extensively studied. Suntivich and Vojvodic et al. have determined surface oxygen binding energy, e_g occupancy, and 3d electron number of transition-metal ions as the activity descriptors of OER in an electrocatalytic water splitting, respectively.[30,31] Unfortunately, these activity descriptors identified in molecule−surface heterogeneous catalysis are not directly transferrable to apply for solid−solid interfacial catalysis, although some OER mechanisms are relevant. Based on first-principles calculations, Kim et al. recently revealed electron-withdrawing surface structures of PtTM(TM = Co, Ti) to have high activity and identified adsorption energies of Li and LiO_2 as catalytic descriptor.[32] However, it is not straightforward to predict that inexpensive compounds with high OER activity by this proposed descriptor.

Very recently, we reported for the first time facet-dependent OER catalytic activity of Co_3O_4 by using first-principles calculations and found the Co_3O_4 octahedron with exposed (111) plane has the higher catalytic activity in reducing charging voltage than (110) and (001) planes.[33] These calculations are in good agreement with experimental measurements.[34−36] Interfacial electrocatalysis has become an attractive point in a rechargable Li-O_2 battery research in order to improve cyclic performance and reduce overpotential in OER. Many transition-metal compounds (TMC: oxide, carbide, and nitride) have been studied as OER catalysts.[17,25,26] Based on these experimental reports and as an extension for our previous Co_3O_4 computational studies, some TMC-catalyzed OER mechanisms are studied in this work in order to identify a descriptor of catalytic activity for OER in Li-O_2 battery. These studies provide a fundamental base for designing a novel and highly active catalyst of OER in the future.

2. COMPUTATIONAL AND EXPERIMENTAL DETAILS

2.1. Computational Methods. First-principles calculations in this work were conducted within the formalism of density functional theory (DFT) and the generalized gradient approximation (GGA) of the exchange−correlation function as formulated by Perdew, Burke, and Ernzerhof (PBE). The valence electron−ion interaction was modeled by the projector augmented wave (PAW) potential implemented in the Vienna ab initio simulation package (VASP).[37,38] The plane wave basis set with a cutoff energy of 450 eV was used. Electron correlation within the d states significantly affects the electronic structure and energetic properties of TMCs. Therefore, the on-site Coulomb correlation effects for 3d orbitals of some transition metals were included in our calculations. According to the previous publications, the effective interaction strengths ($U_{eff} = U - J$) of different 3d orbitals were set as 2.5 = 2.5−0.0 for Ti atom in TiO, $TiCl_3$, TiN, and TiC,[39] 4.0 = 5.0−1.0 for Mn atom in MnO and Mn_2O_3,[40] 6.4 = 7.4−1.0 for Ni atom in NiO,[40] 3.3 = 3.8−0.5 for Co atom in CoO,[40] 2.0 = 2.0−0.0 for Co atom in Co_3O_4,[33] 3.6 = 4.5−0.9 for Fe atom in Fe_3O_4,[41] and 4.0 = 5.0−1.0 for Zn atom in ZnO,[42] in which U is on-site Hubbard repulsion and J is Hund's exchange interaction. The calculated total energies are insensitive to J when U_{eff} is fixed. Plain PBE (U_{eff} = 0.0) was applied in Mo_2C and MoS_2 systems based on the previous publications.[43,44] Our plain PBE and PBE+U test calculations based on these parameters were in fair agreement with experimental band gaps and bulk lattice parameters. The surface Brillouin zone was sample with the K-points generated by the Monkhorst−Pack scheme with a space <0.05 $Å^{-1}$. The structures have been relaxed until a maximum force of <0.02 eV/Å and the energy convergence criterion is 10^{-4} eV. These set parameters were confirmed for accuracy and effectiveness by comparing with experimental data used in our previous calculations.[33,45,46]

For the well-known overbinding of the O_2 molecular with DFT, the energy of O_2 molecule is determined by the formula of $H(T = 0\ K, O_2) = 2H(T = 0\ K, O) - \Delta E^{exptl}$,[47] where ΔE^{exptl} (5.12 eV) is the binding energy of O_2, $H(T = 0, X)$ is the calculated ground state of oxygen atom (X = O) or oxygen molecular ($X = O_2$).[48] The free energy of O_2 which includes the enthalpic contributions of $7/2k_BT$ is due to translational, rotational, and PV degrees of freedom, while the entropic contributions are taken from tabulated experimental data. Based on experimental thermodynamic data of bulk Li_2O_2 and Li,[48] we calculated open-circuit potential of $2Li^+ + O_2 + 2e^- \leftrightarrow Li_2O_2$ to be 2.98 V, which is quite close to the experimental value (2.96 V). The calculated formation enthalpy and Gibbs energy of Li_2O_2 are −6.57 eV and −5.96 eV, respectively, which are in good agreement with the experimental data (−6.57 eV and −5.92 eV).[48]

The first-principles thermodynamic model is applied to describe charging process of Li-O_2 battery, as follows:

$$\Delta G = [E - E_0 + \Delta N_{Li}(\mu_{Li} - eV_c) + \Delta N_{O_2}\mu_{O_2}] \quad (1)$$

where E is the final energy of a certain step, E_0 is the initial energy, ΔN_{Li} and ΔN_{O_2} are the number of the Li and O_2 that is removed. V_c is the electromotive force corresponding to charging voltage when OER occurs spontaneously ($\Delta G < 0$). The V_c value is determined on the basis of $\Delta G < 0$ for all intermediates in the reaction path. The definition reflects the energy conservation in a multistep chemical reaction which is nothing special in electrochemical reaction. This computational model was also used in the Li_2O_2 OER mechanism calculated by Mo et al.[49]

2.2. Materials Synthesis. All the reagents were of analytical purity and were used without further purification. Co_3O_4 nanoparticles were synthesized through hydrothermal process. In a typical synthesis, 4 mmol $Co(Ac)_2{\cdot}4H_2O$ was dissolved in 80 mL distilled water with magnetic stir for 30 min, then sealed, maintained at 180 °C for 12 h, and allowed to cool to room temperature. The product was centrifuged, washed with distilled water and ethanol several times, and finally dried at 80 °C for 6h. CoO nanoparticles were synthesized with the similar process except the usage of solvent ethanol.

2.3. Electrochemical Measurements of Li-O_2 Cell. The electrodes were formed by casting a ball-milled slurry mixture of the synthesized catalyst, Ketjen black carbon (KB), and polyvinylidene fluoride (PVDF) onto a nickel foam. The electrochemical cells used were based on a Swagelok Cell design composed of a Li metal anode, an electrolyte LiTFSI in TEGDME, the Celgard 2400 separator (16 mm in diameter), and the as-prepared porous cathode. The cells were assembled in a glovebox with oxygen and water contents <1 ppm.

3. RESULTS AND DISCUSSION

3.1. Interfacial Catalytic Model. To determine the catalytic activity of different TMC surfaces, a reference of energy level must be obtained by calculating OER mechanism in $(1\bar{1}00)$ surface of Li_2O_2. The selected surface is very likely exposed after discharging because of the low surface energy of Li_2O_2 $(1\bar{1}00)$ calculated by Radin et al.[47] More importantly, Li^+ and O_2 desorption energies on Li_2O_2 $(1\bar{1}00)$ surface can make a consistent comparison with those on TMC-catalyzed Li_2O_2 $(1\bar{1}00)$ surface in the following discussion (TMC-Catalyzed OER Mechanisms section). The calculated energy profile and structural evolution of $Li^+ \rightarrow Li^+ \rightarrow O_2$ are displayed in Figure 1. The charging voltage and desorption energy of rate-determinant step (O_2 desorption) are calculated as 3.23 V and 1.75 eV in terms of $Li^+ \rightarrow Li^+ \rightarrow O_2$ pathway, respectively. These values can be regarded as references to evaluate catalytic activity of TMO in the interface of TMC/Li_2O_2/O_2.

DOI: 10.1021/jacs.5b07792
J. Am. Chem. Soc. 2015, 137, 13572−13579

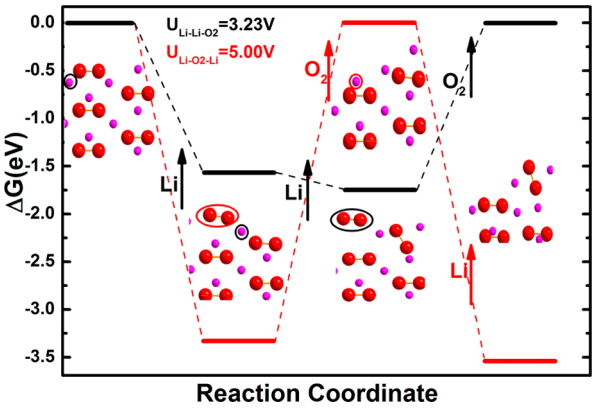

Figure 1. Energy profiles of possible OER paths starting from Li_2O_2 $(1\bar{1}00)$ surface. The charge voltage for $Li^+ \rightarrow Li^+ \rightarrow O_2$ and $Li^+ \rightarrow O_2 \rightarrow Li^+$ are 3.23 and 5.00 V, respectively.

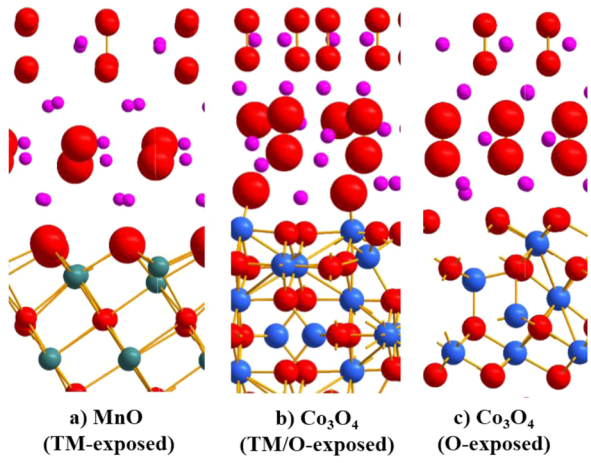

Figure 2. Relaxed interfacial structures between the Li_2O_2 (0001) and TMO surfaces with different composition, TM-rich, TM/O-co-existence, and O-rich. The red, pink, blue, green balls represent oxygen, lithium, cobalt, and manganese atoms, respectively. Specifically, the bigger red balls represent oxygen atoms from Li_2O_2 in the interface.

According to *in situ* TEM experimental observation, Shao-Horn et al. elucidated that OER mainly takes place in the three-phase interface of cathode/Li_2O_2/electrolyte.[50] As such, TMC/Li_2O_2/O_2 interfacial model in the present study is constructed to simulate catalytic activity in reducing charging overpotential and desorption energies of O_2 and Li^+. Such a computational model was successfully applied to calculate OER catalytic mechanism of Co_3O_4/Li_2O_2/O_2 system.[33] The calculated discharging−charging overpotentials and catalytic activities of specific surfaces were consistent with experimental measurements by two research groups.[34,35] In fact, constructing a rational interfacial model plays a critical role in determining catalytic activity of TMC. According to the first-principles thermodynamic calculations for Li_2O_2, Radin et al. identified that Li_2O_2 (0001) and $(1\bar{1}00)$ surfaces are very likely to be exposed after discharging,[47] which was later confirmed by Shao-Horn et al.[51] Therefore, in our interfacial model, two O-rich surfaces (0001) and $(1\bar{1}00)$ are exposed in vacuum to simulate the O_2 gas environment. The Li_2O_2 (0001) with the lowest surface energy is considered to directly interact with catalyst surface, while the Li_2O_2 $(1\bar{1}00)$ is exposed in vacuum. The O_2 and Li^+ desorption on the TMC-catalyzed Li_2O_2 $(1\bar{1}00)$ is calculated in order to compare with those on pure Li_2O_2 $(1\bar{1}00)$. The third dimension of Li_2O_2 is calculated periodically.

It is of great importance to determine which TMC surface should directly interact with Li_2O_2 (0001). Our previous studies indicate that O-rich Co_3O_4 (111) surface has the highest catalytic activity to enhance Li^+ and O_2 desorption by attracting electrons of Li_2O_2,[33] while Co/O-co-existence Co_3O_4 (110) surface lead to Li_2O formation and has much higher Li^+ and O_2 desorption energies, which was later confirmed by two research groups.[34,35] Further, the typical surface structures with different compositions, TM-rich, TM/O-co-existence, and O-rich, were directly interfaced with Li_2O_2 in order to select a high active catalytic surface for specific TMC. The relaxed interfacial structures of Li_2O_2(001)/TMC-surfaces were presented in Figure 2. Our calculations indicate that TM-exposed surfaces, TM-rich and TM/O-co-existence, directly result in Li_2O formation. The previous experimental and theoretical studies showed that OER of Li_2O requires a high charging voltage.[33,52] Only O-rich surface can make Li_2O_2 maintain O_2^{n-} state and avoid Li_2O formation.

In fact, a significant reconstruction of catalytic surface structure usually takes place in catalytic reaction processes. The steady-state catalytic performance should be evaluated based on surface restructured form rather than initial bulk surface phase.[53] Very recently, Curtiss et al. reported that Mo_2C/CNT had a high catalytic activity in increasing electrical efficiency and cycle life.[43] The analysis for surface structures indicates that formation of noncystalline MoO_3-like layers on the Mo_2C plays an important role in reducing charging voltage. In 2013, Thotiyl et al. prepared a stable TiC-based cathode material which exhibits a great electrochemical performance in reversibility, reducing side reactions, and energy capacity.[26] The stability and high electrochemical performance are attributed to surface reconstruction, forming TiOC structure. Indeed, a metal-exposed surface is not stable in a high O_2 concentration and gradually converts into nonmetal-exposed surface. Our recent calculations indicated that such O/C-exposed surface has enhanced ability in reducing charging voltage. Therefore, our interfacial models in this work are based on nonmetal-exposed surfaces of TMC.

The interfacial structure of Li_2O_2/TMC was optimized to obtain the smallest lattice mismatch of two solid phases. The detailed procedure of interfacial structure calculations has been elaborately described in our previous paper.[33] The calculated interfacial structures of Li_2O_2/TMC (TMC = MnO, TiO, ZnO, NiO, MoS_2, TiN, and $TiCl_2$) were presented in Figure S1 (Supporting Information).

3.2. TMC-Catalyzed OER Mechanisms. In our previous works, we have calculated all possible pathways, namely $Li^+ \rightarrow Li^+ \rightarrow O_2$, $O_2 \rightarrow Li^+ \rightarrow Li^+$, and $Li^+ \rightarrow O_2 \rightarrow Li^+$ on Co_3O_4 surfaces and X-doped graphene (X = B, N, Al, Si, P, and S).[33,45,46] These studies indicated that $Li^+ \rightarrow Li^+ \rightarrow O_2$ was the thermodynamically lowest-energy pathway for OER, and O_2 evolution was the rate-determinant step. The process can be described as the stepwise Li^+ desorption and O_2 evolution from nanoscale Li_2O_2. The desorption order in $Li^+ \rightarrow Li^+ \rightarrow O_2$ pathway directly reduces the amount of Li−O bonds, which favors decreasing the O_2 evolution barrier. $O_2 \rightarrow Li^+ \rightarrow Li^+$ and $Li^+ \rightarrow O_2 \rightarrow Li^+$ pathways require surmounting the higher activation barriers than $Li^+ \rightarrow Li^+ \rightarrow O_2$. Therefore, as an extension of Li_2O_2/Co_3O_4, it is rationally predicted that $Li^+ \rightarrow Li^+ \rightarrow O_2$ is very likely to be the lowest-energy pathway in X-doped graphene, and hence other pathways such as $O_2 \rightarrow Li^+$

DOI: 10.1021/jacs.5b07792
J. Am. Chem. Soc. 2015, 137, 13572−13579

→ Li^+ and $Li^+ \rightarrow O_2 \rightarrow Li^+$ are not considered in the present studies.

Based on the established interfacial models of Li_2O_2/TMC, we calculated their $Li^+ \rightarrow Li^+ \rightarrow O_2$ reaction paths. Based on eq 1, the corresponding charging voltages are estimated with the spontaneous electrochemical reaction condition of $\Delta G \leq 0$. For simplicity, only $O_2 \rightarrow Li^+ \rightarrow Li^+$ reaction path of Li_2O_2/NiO and the corresponding structural evolution are presented in Figure 3. The other reaction paths and structural evolutions are

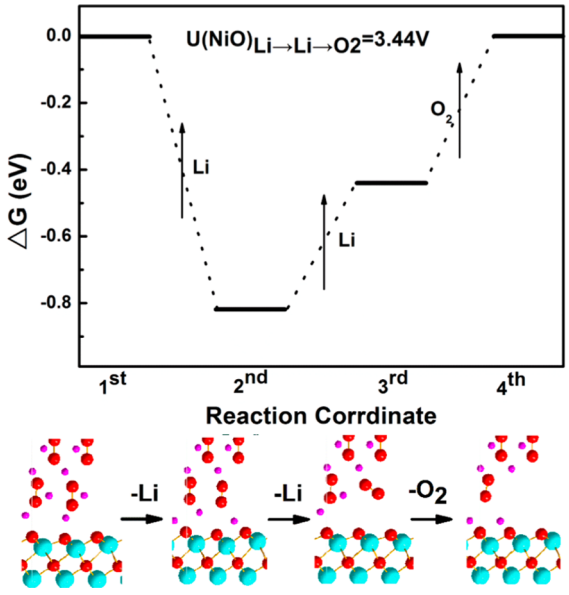

Figure 3. Calculated energy profiles and structural evolutions of $Li^+ \rightarrow Li^+ \rightarrow O_2$ reaction paths of Li_2O_2 OER on NiO. Small pink, medium red, and large light blue balls represent Li, O, and Ni, respectively.

given in Figure S2. The detailed thermodynamic data such as charging voltages and desorption energies of Li^+ and O_2 are summarized in Table 1. Under external voltage, O_2 desorption step is determined as the rate-determinant step of OER in all these catalytic systems due to the highest desorption barrier.

Table 1. Desorption Energies (eV) of Lithium atoms and O_2 molecular and Charging Voltage (V) of Different TMCs

	first Li	second Li	average Li	O_2	voltage
TiO	2.71	2.60	2.65	1.50	3.40
MnO	0.93	3.31	2.12	0.95	2.59
Co_3O_4	1.60	2.52	2.06	1.27	2.69
NiO	2.62	3.82	3.22	0.43	3.44
ZnO	3.06	3.72	3.39	0.56	3.67
MoS_2	2.61	3.21	2.91	1.05	3.44
$TiCl_3$	2.58	2.90	2.74	1.84	3.66
TiN	1.96	1.92	1.94	1.74	2.81

As shown in Table 1, there is an opposite trend between desorption energies of Li^+ and O_2. For example, a low O_2 desorption energy of 0.43 eV corresponds to a high average Li^+ desorption energy of 3.22 eV, while a high O_2 desorption energy of 2.14 eV corresponds to a low average Li^+ desorption energy of 1.74 eV. After carefully observing the structural difference of these reactions, we found that a high Li^+ desorption energy is usually attributed to a strong electrostatic attraction between Li^+ and catalytic surface because they have a closer distance. In this case, the charge analysis indicates that a large charge transfer has undergone from O_2^{2-} to catalytic surface. As such, the O_2^{2-n} species after electron transfer has a low O_2 desorption energy. In conclusion, the charge transfer plays a critical role in determining catalytic activity of TMC. When the size and morphology of Li_2O_2 are very similar, the electron-withdrawing abilities of catalytic surfaces become a determinant factor. It is very necessary to quantitatively describe an optimum electron-withdrawing ability of catalytic surface to reduce charging overpotential and O_2 desorption energy barrier.

3.3. Descriptor of Catalytic Activity. Based on established catalytic mechanisms of OER in Li-O_2, it is necessary to identify a convenient activity descriptor to accelerate screening of highly active catalysts. The previously identified catalytic activity descriptors in electrocatalytic water-splitting OER may not be directly transferrable in OER of Li-O_2 battery because of completely different catalytic mechanisms.[30,54] Although Kim et al. identified adsorption energies of Li and LiO_2 as catalytic activity descriptor, there may be some limitations due to only PtCo and PtTi compounds involved in their studies.[32] More importantly, the adsorption energies for ions and radical may not directly apply in catalyst screening in experiments.

Our previous Co_3O_4 studies showed that catalytic activity in reducing charging voltage and O_2 evolution barrier is strongly associated with surface Lewis acidity which is typically defined by electron attraction ability of a specific catalytic site.[33] Very recently, Kim et al. also made a conclusion that an electron-withdrawing surface structure has a high catalytic activity in reducing charging voltage.[32] It is necessary to extend this concept of Lewis acidity from catalytic site to whole surface structure because a large number of transferred electrons are dispersed into catalytic surface through solid−solid interfacial interaction. As such, the surface acidity (V_{sa}) of catalyst is defined by the following equation:

$$V_{sa} = \frac{S_0}{S}\frac{E_{Q_0+qS/S_0} - E_{Q_0}}{e} \quad (2)$$

Where E_{Q_0} is the total energy of specific surface of catalyst; Q_0 is the number of electrons of the neutral surface model, and q refers to the number added in per surface area. As a result, E_{Q_0+qS/S_0} is total energy of a surface model in which the certain electrons are added; S is area of the surface model and S_0 is the specific surface area. For consistency, five layers of surface models were used in our present calculations. The definition of acidity directly describes the electron-withdrawing capability of surface structure, which is in essence consistent with electron affinity of atom and molecular models.

To quantitatively describe the relationship of desorption energies of O_2 and Li^+ and charging voltage with surface acidity, the calculated values of TiO, NiO, MnO, ZnO, MoS_2, Co_3O_4, TiN, and $TiCl_3$ are used to roughly fit their correlation. As shown in Figure 4, O_2 desorption barrier shows linear correlation with surface acidity, indicating that electron transfer from Li_2O_2 to catalytic surface favors reducing O_2 desorption energy. However, the Li^+ desorption energies present a second-order curve (red line) with surface acidity. The lowest Li^+ desorption energy corresponds to the surface acidity of 2.25 V according to our definition. Similarly, based on the calculated values in Table 1, a second-order curve is presented to describe the correlation of charging voltage with surface acidity, which is

DOI: 10.1021/jacs.5b07792
J. Am. Chem. Soc. 2015, 137, 13572−13579

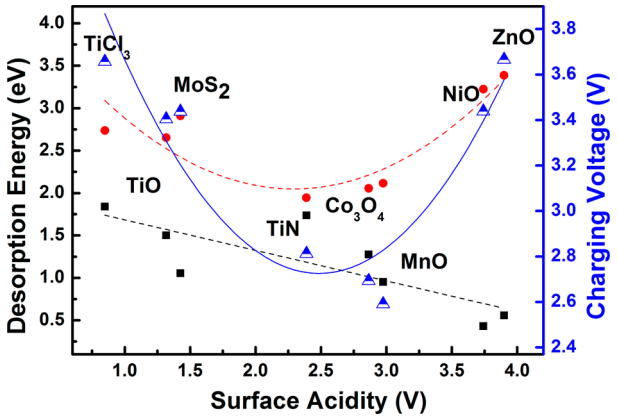

Figure 4. Desorption energies (eV) of Li^+ and O_2, and charging voltage (V) versus surface acidity. The red, blue, and black lines drawn with the acidity strength of 0.5−4.0 V roughly exhibit the change trends of charging voltage and desorption energies as a function of surface acidity.

consistent with the trend of integrated Li^+ and O_2 desorption energies. It is worth pointing out that the main goal of our present calculations is to identify an optimal value of surface acidity rather than focusing on exact values of desorption energy and charging voltage.

In nature, the surface acidity descriptor proposed in this study established a quantitative characterization on electron exchange capability between two species in solid−solid interface. The concept of surface acidity is consistent with electron affinity (EA), which is widely used to describe electron-withdrawing capability of atom or molecule. Certainly, the electron exchange plays an important role in the catalytic activation of chemical bonds. In addition, the interface structure in which vacancies and polarons usually are generated by interfacial mismatch may be an important factor to affect catalytic activity. As such, we expect that the surface acidity model should apply to any catalytic systems in which catalytic activity is dominated by electron exchange rather than interface structure. Developing a highly efficient model including electron exchange and interface structure is under way.

In the past decade, several catalytic descriptors including d-band center,[1−9] specific orbital number,[30,31] and adsorption energy[23,28,29] have been established to correlate catalytic activity. However, these models mostly describe the interaction between localized catalytic site and gas molecule. In contrast, the surface acidity model has a significant advantage in describing the delocalized solid−solid interface interaction. However, measuring a delocalized surface acidity accurately in experiment and theory is not established so far.

3.4. Predicting Active Catalysts for OER. As shown in eq 1, the thermodynamic overpotentials are considered in the present studies. This implies that lithium ions in aprotic solution are in equilibrium ($Li \leftrightarrow Li^+ + e^-$) with lithium metal anode and with Li^+ near cathodes surface. This is a concerted process of Li^+-migration coupled with electron transfer under charging potential. In this instance, the Li^+ desorption kinetic behavior from solid to solution is not necessary to be considered. The previous success of thermodynamic overpotential in describing OER onset electrochemical currents indicates such an approximation is rational with a valid description of onset potentials. According to Figure S2, the O_2 desorption energies are higher than those of Li^+ under charging potential in most TMC catalysts. Therefore, the O_2 desorption energy and charging voltage are used to evaluate catalytic activity in our predictive calculations.

In order to predict the possible highly active catalysts for OER in Li-O_2 battery, the correlation curves of O_2 desorption energy and charging voltage with surface acidity are exhibited in Figure 5. Further the acidity of nonmetal-exposed surfaces of

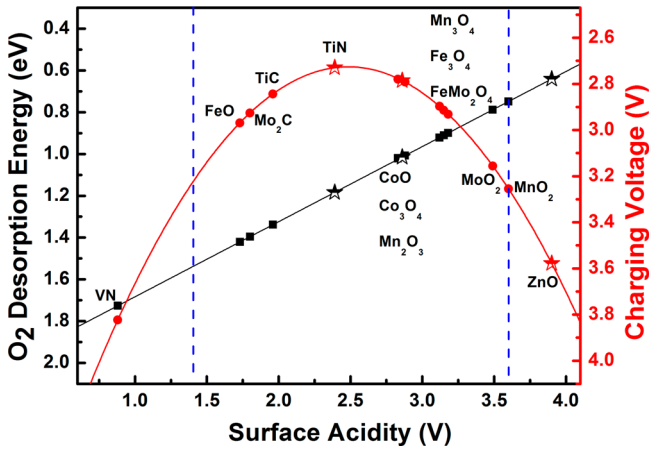

Figure 5. Predicted catalytic activities of some TMCs based on the established correlation of O_2 desorption and charging voltage with surface acidity. All values were calculated based on surface acidity, although charging voltages and O_2 desorption energies of TiN, Co_3O_4, and ZnO have been calculated before.

potential TMC catalysts is obtained by the first-principles calculations and eq 2. In terms of charging voltage, the catalytic activity presents a volcano correlation with surface acidity. However, O_2 desorption energies have linear correlation with surface acidity. Based on our OER mechanism of pure Li_2O_2 (Figure 1), the lowest-energy reaction path has the O_2 desorption energy and charging voltage of 1.75 eV and 3.23 V, respectively. Therefore, the TMC compounds whose acidity is between 1.4 and 3.6 V (two blue dash lines) should have catalytic activity. Combining O_2 desorption energy and charging voltage, we predict that these compounds with surface acidity of 2.4−3.1 V should have the highest catalytic activity.

Based on Figure 5, some TMCs such as TiN, CoO, Co_3O_4, Mn_2O_3, Mn_3O_4, Fe_3O_4, $FeMn_2O_4$, and MoO_2 are predicted as possible highly active OER catalysts in Li-O_2 battery. Again, it is emphasized that nonmetal-exposed surface structures play an important role in reducing O_2 desorption energy and charging voltage. In the charging conditions, Curtiss and Thotiyl established the surface oxidation mechanism of Mo_2C and TiC as cathodes.[26,52] More importantly, they characterized that nascent MoO_3 and TiOC surface structures play an important role in reducing charging voltage and improving cyclic performance. It is expected that oxidized surface structures become stronger in acidity. Therefore, we reasonably predict Mo_2C and TiC are highly active catalysts for OER in Li-O_2 battery. Relatively, catalytic activities of TMOs are closer to experimental characterizations because O-exposed surface structures were used in our OER mechanisms.

3.5. Experimental Confirmation. It is important to compare the result obtained based on theoretical calculations with those reported from experimental characterization. Our calculations indicate that TMOs such as CoO, Co_3O_4, Fe_3O_4, Mn_3O_4, and Mn_2O_3 may have a high catalytic activity in

DOI: 10.1021/jacs.5b07792
J. Am. Chem. Soc. 2015, 137, 13572−13579

reducing charging voltage and O_2 desorption energy. Co_3O_4 supported on carbon and metal cathodes has been extensively studied as an OER catalyst. It exhibits a superior catalytic performance in reducing ~0.6 V overpotential and improving cyclic stability, which is in good agreement with our previous mechanism studies and current prediction. CoO is predicted to have high catalytic activity which is comparable with that of Co_3O_4 according to our calculated prediction. However, no experimental study on CoO catalytic activity in Li-O_2 cell is reported so far.

In order to confirm our calculated prediction, a comparative experiment on electrochemical performance of CoO and Co_3O_4 in similar conditions was carried out. The XRD patterns of the synthesized Co_3O_4 and CoO nanoparticles are shown in the Figure 6. All peaks in these XRD patterns can be indexed to

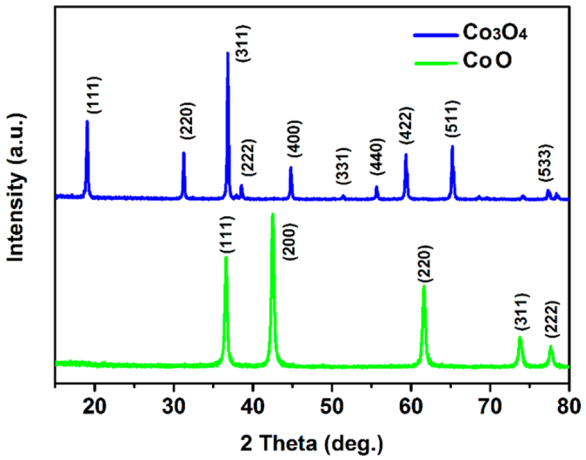

Figure 6. XRD patterns of the prepared Co_3O_4 (top, blue) and CoO (below, green) powder.

Co_3O_4 (JCPDS card no. 42-1467) and CoO (JCPDS card no. 48-1719). As shown in Figure 6, the facet (111) is the second possible exposed surface in both Co_3O_4 and CoO systems, which is qualitatively consistent with the selected surface in our calculations. The TEM images of the synthesized Co_3O_4 and CoO nanoparticles are displayed in Figure 7a,b, respectively. The prepared Co_3O_4 (~50 nm) has a slightly larger particle size than CoO (~40 nm), exhibiting a similar cubic morphology of both nanoparticles.

At the same current density (0.1 mA·cm^{-2}) and limited discharge capacity (1000 mAh·g^{-1}), the catalytic effect of Co_3O_4 and CoO on the discharge and charge voltage of Li-O_2 cells was examined, as shown in Figure 8a,b, respectively. The discharge voltages of two cells are very similar and are stabilized at 2.75 V. There are two charge plateaus, 3.5 and 4.05 V, in Li-

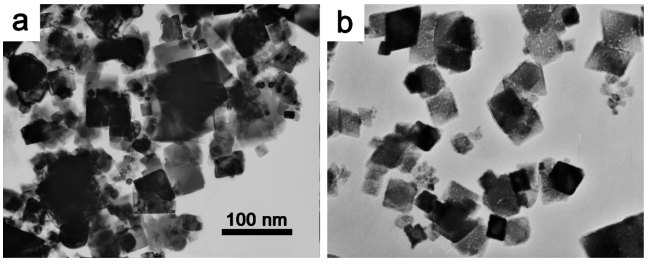

Figure 7. TEM images of the synthesized Co_3O_4 (a) and CoO (b) nanoparticles.

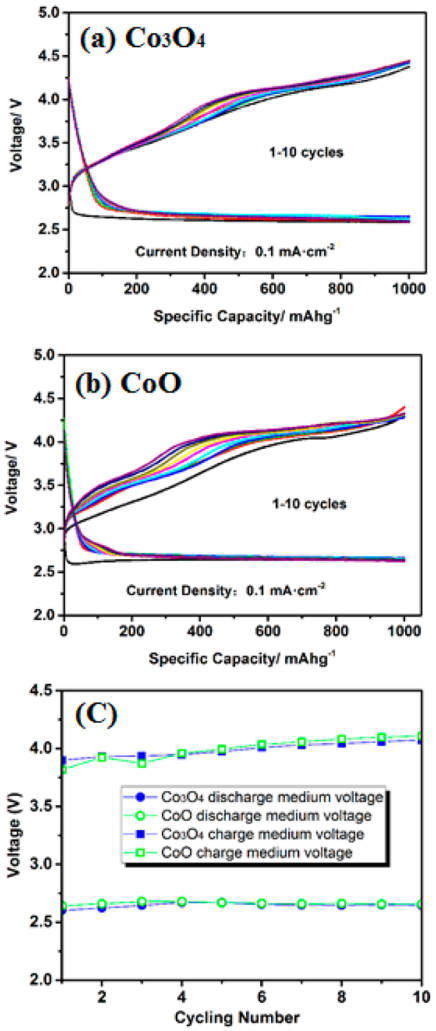

Figure 8. Discharging and charging profiles of the Co_3O_4 (a) and CoO (b); the variation of discharge and charge medium voltage with the cycle number (c) when the capacity is limited to 1000 mAh·g^{-1}.

O_2 cells catalyzed by Co_3O_4 and CoO. However, the initial charge voltage of CoO is obviously lower than that of Co_3O_4. With the cycles increased, two cells reach a very similar electrochemical performance in discharge and charge voltage. It indicates that the clean CoO (111) surface may have a slightly higher (or very similar) catalytic activity than that of Co_3O_4, which is very consistent with our predicted calculation.

Transition-metal carbides and nitride Mo_2C, TiC, and TiN were studied as Li-O_2 cathodes and exhibited a significantly low charging potentials and good cyclic performance.[25,26,43] As an efficient bifuncational catalyst, TiN nanoparticles supported on carbon materials were found to have an excellent catalytic effect on OER, a significantly low onset potential of 2.9 V, and reducing about 0.45 V discharging-charging gap.[25] This experimental result is consistent with our present calculations. The structural characterization indicates that surface oxidation takes place in TiC and Mo_2C, forming TiOC and MoO_3 species, which are responsible for low charging overpotential and high capability.[26,43] In Mo_2C, the charging voltage was stabilized in 3.25−3.4 V with a cycle life more than 100 times.[43] These experimental and computational results are consistent with our current prediction. Our very recent calculations also show that TiC surfaces covered by a certain percentage of O

DOI: 10.1021/jacs.5b07792
J. Am. Chem. Soc. 2015, 137, 13572−13579

can enhance thermodynamic stability of surface structure and reduce charging potential. The related experimental work is underway with an aim to elucidate the catalytic activity of O-covered TiC and Mo_2C.

Besides the role of exposed O, catalytic activity is also capable to be tailored by solid-solution treatment of cations, forming multivalence sites like Co_3O_4. The previous studies indicate that the edge-sharing octahedral spinels with multivalence 3d transition metals exhibit superior OER catalytic activity which is comparable with IrO_2 and RuO_2.[55,56] Indeed, the variable valence states of cations are favorable to electron transfer between Li_2O_2 and catalysts.

Finally, it is important to define an observable parameter in experiment to determine surface acidity. The surface acidity describes the electron-withdrawing capacity of catalyst, which in nature corresponds to desorption energy of catalyzed species. In experiment, it is very difficult to measure electron-exchange amount and binding strength of solid−solid interface. Therefore, we propose that desorption energy of NH_3 is used to characterize surface acidity of catalyst. A larger desorption energy corresponds to a stronger surface acidity. Desorption energies of NH_3 on different surfaces can be easily obtained in experiment and theory. Based on NH_3 desorption, the electron-withdrawing capacity of catalyst can be quantitatively characterized. It should be pointed out that gas−solid heterogeneous catalysis may have a little difference from solid−solid interface catalysis. The NH_3 desorption energy of Co_3O_4 is calculated as 1.43 eV, which means any catalyst with NH_3 desorption energy of approximative 1.43 eV may show good catalytic activity for OER in Li-O_2 battery. As shown in Figure S3, our charge density difference analysis exhibits electron transfer from NH_3 to Co_3O_4.

4. CONCLUSIONS

In this study, we proposed a model of surface acidity that is correlated with interfacial catalytic activity in reducing charging overpotential and O_2 evolution barrier in OER of Li-O_2 battery. The surface acidity is defined to describe the electron-withdrawing ability of catalysts in a large area of interfacial reaction and can be characterized by NH_3 desorption energy. We found that charging voltage exhibits volcano correlation with surface acidity and the highest catalytic activity corresponding to NH_3 desorption energy of 1.43 eV. Several TMCs (Co_3O_4, TiC, TiN) with high catalytic activity have been confirmed by the previous experimental studies. CoO is predicted to have as high a catalytic activity as Co_3O_4 in reducing charging overpotential, which is further confirmed by our comparative electrochemical experiment in a similar condition. It is emphasized that the catalytic descriptor was established based on nonmetal-exposed surface structures of TMCs. The metal-exposed surface structures are very likely to convert into O-covered surface during the ORR/OER cycles. Therefore, the established catalytic descriptor should be applied in a steady-state reconstructed surface structures.

■ ASSOCIATED CONTENT

Supporting Information

The Supporting Information is available free of charge on the ACS Publications website at DOI: 10.1021/jacs.5b07792.

Calculated interfacial models of Li_2O_2 supported on TiO, MnO, Co_3O_4, NiO, ZnO, TiN, $TiCl_3$ and MoS_2; calculated energy profiles of Li_2O_2 decomposition reactions along $Li^+ \rightarrow Li^+ \rightarrow O_2$ path catalyzed by TiO, MnO, ZnO, MoS_2, TiN, and $TiCl_3$; charge density difference of NH_3 supported on Co_3O_4 (111) surface with respect to NH_3 and Co_3O_4 (PDF)

■ AUTHOR INFORMATION

Corresponding Authors

*jliu@mail.sic.ac.cn
*zywen@mail.sic.ac.cn
*wqzhang@mail.sic.ac.cn

Notes

The authors declare no competing financial interest.
[‖]These authors contributed equally.

■ ACKNOWLEDGMENTS

This work is financially supported by "One-Hundred-Talent Project", "the Key Research Program (grant no. KGZD-EW-T06)" of the Chinese Academy of Sciences, National Natural Science Foundation of Chinese, NSFC (51432010, 21573272), and the research grant (no. 14DZ2261200) from Shanghai government. In addition, Prof. B. V. R. Chowdari (Department of Physics, National University of Singapore) is greatly acknowledged for helpful discussion.

■ REFERENCES

(1) Hammer, B.; Norskov, J. K. *Advances in Catalysis*; Elsevier: Amsterdam, The Netherlands, 2000; Vol *45*, p 71 10.1016/S0360-0564(02)45013-4
(2) Huo, C. F.; Li, Y. W.; Wang, J. G.; Jiao, H. J. *J. Am. Chem. Soc.* **2009**, *131*, 14713.
(3) Ruban, A.; Hammer, B.; Stoltze, P.; Skriver, H. L.; Norskov, J. K. *J. Mol. Catal. A: Chem.* **1997**, *115*, 421.
(4) Lu, C.; Lee, I. C.; Masel, R. I.; Wieckowski, A.; Rice, C. *J. Phys. Chem. A* **2002**, *106*, 3084.
(5) Kitchin, J. R.; Norskov, J. K.; Barteau, M. A.; Chen, J. G. *J. Chem. Phys.* **2004**, *120*, 10240.
(6) Stamenkovic, V.; Mun, B. S.; Mayrhofer, K. J. J.; Ross, P. N.; Markovic, N. M.; Rossmeisl, J.; Greeley, J.; Norskov, J. K. *Angew. Chem., Int. Ed.* **2006**, *45*, 2897.
(7) Norskov, J. K.; Bligaard, T.; Rossmeisl, J.; Christensen, C. H. *Nat. Chem.* **2009**, *1*, 37.
(8) Xin, H. L.; Linic, S. *J. Chem. Phys.* **2010**, *132*, 221101.
(9) Greeley, J.; Stephens, I. E. L.; Bondarenko, A. S.; Johansson, T. P.; Hansen, H. A.; Jaramillo, T. F.; Rossmeisl, J.; Chorkendorff, I.; Norskov, J. K. *Nat. Chem.* **2009**, *1*, 552.
(10) Shao, Y. Y.; Ding, F.; Xiao, J.; Zhang, J.; Xu, W.; Park, S.; Zhang, J. G.; Wang, Y.; Liu, J. *Adv. Funct. Mater.* **2013**, *23*, 987.
(11) Girishkumar, G.; McCloskey, B.; Luntz, A. C.; Swanson, S.; Wilcke, W. *J. Phys. Chem. Lett.* **2010**, *1*, 2193.
(12) Cheng, F. Y.; Chen, J. *Chem. Soc. Rev.* **2012**, *41*, 2172.
(13) Li, F. J.; Zhang, T.; Zhou, H. S. *Energy Environ. Sci.* **2013**, *6*, 1125.
(14) Peng, Z. Q.; Freunberger, S. A.; Chen, Y. H.; Bruce, P. G. *Science* **2012**, *337*, 563.
(15) Jung, H. G.; Hassoun, J.; Park, J. B.; Sun, Y. K.; Scrosati, B. *Nat. Chem.* **2012**, *4*, 579.
(16) Christensen, J.; Albertus, P.; Sanchez-Carrera, R. S.; Lohmann, T.; Kozinsky, B.; Liedtke, R.; Ahmed, J.; Kojic, A. *J. Electrochem. Soc.* **2012**, *159*, R1.
(17) Débart, A.; Bao, J.; Armstrong, G.; Bruce, P. G. *J. Power Sources* **2007**, *174*, 1177.
(18) Debart, A.; Paterson, A. J.; Bao, J.; Bruce, P. G. *Angew. Chem., Int. Ed.* **2008**, *47*, 4521.
(19) Cheng, H.; Scott, K. *J. Power Sources* **2010**, *195*, 1370.
(20) Mizuno, F.; Nakanishi, S.; Kotani, Y.; Yokoishi, S.; Iba, H. *Electrochemistry* **2010**, *78*, 403.

DOI: 10.1021/jacs.5b07792
J. Am. Chem. Soc. 2015, 137, 13572−13579

(21) Read, J. *J. Electrochem. Soc.* **2002**, *149*, A1190.
(22) Zhang, G. Q.; Zheng, J. P.; Liang, R.; Zhang, C.; Wang, B.; Hendrickson, M.; Plichta, E. J. *J. Electrochem. Soc.* **2010**, *157*, A953.
(23) Lu, Y. C.; Xu, Z. C.; Gasteiger, H. A.; Chen, S.; Hamad-Schifferli, K.; Shao-Horn, Y. *J. Am. Chem. Soc.* **2010**, *132*, 12170.
(24) Sun, B.; Munroe, P.; Wang, G. X. *Sci. Rep.* **2013**, *3*, 2247.
(25) He, P.; Wang, Y. G.; Zhou, H. S. *Chem. Commun.* **2011**, *47*, 10701.
(26) Thotiyl, M. M. O.; Freunberger, S. A.; Peng, Z. Q.; Chen, Y. H.; Liu, Z.; Bruce, P. G. *Nat. Mater.* **2013**, *12*, 1050.
(27) Shui, J. L.; Karan, N. K.; Balasubramanian, M.; Li, S. Y.; Liu, D. J. *J. Am. Chem. Soc.* **2012**, *134*, 16654.
(28) Xu, Y.; Shelton, W. A. *J. Chem. Phys.* **2010**, *133*, 024703.
(29) Dathar, G. K. P.; Shelton, W. A.; Xu, Y. *J. Phys. Chem. Lett.* **2012**, *3*, 891.
(30) Suntivich, J.; May, K. J.; Gasteiger, H. A.; Goodenough, J. B.; Shao-Horn, Y. *Science* **2011**, *334*, 1383.
(31) Vojvodic, A.; Norskov, J. K. *Science* **2011**, *334*, 1355.
(32) Kim, H.-J.; Jung, S. C.; Han, Y.-K.; Oh, S. H. *Nano Energy* **2015**, *13*, 679.
(33) Zhu, J. Z.; Ren, X. D.; Liu, J. J.; Zhang, W. Q.; Wen, Z. Y. *ACS Catal.* **2015**, *5*, 73.
(34) Gao, R.; Zhu, J. Z.; Xiao, X. L.; Hu, Z. B.; Liu, J. J.; Liu, X. F. *J. Phys. Chem. C* **2015**, *119*, 4516.
(35) Su, D. W.; Dou, S. X.; Wang, G. X. *Sci. Rep.* **2014**, *4*, 5767.
(36) Cui, Y. M.; Wen, Z. Y.; Liu, Y. *Energy Environ. Sci.* **2011**, *4*, 4727.
(37) Kresse, G.; Hafner, J. *Phys. Rev. B: Condens. Matter Mater. Phys.* **1993**, *47*, 558.
(38) Kresse, G.; Furthmuller, J. *Comput. Mater. Sci.* **1996**, *6*, 15.
(39) Stausholm-Møller, J.; Kristoffersen, H. H.; Hinnemann, B.; Madsen, G. K. H.; Hammer, B. *J. Chem. Phys.* **2010**, *133*, 144708.
(40) Wang, L.; Maxisch, T.; Ceder, G. *Phys. Rev. B: Condens. Matter Mater. Phys.* **2006**, *73*, 195107.
(41) Kiejna, A.; Ossowski, T.; Pabisiak, T. *Phys. Rev. B: Condens. Matter Mater. Phys.* **2012**, *85*, 125414.
(42) Karmakar, D.; Rao, T. V. C.; Yakhmi, J. V.; Yaresko, A.; Antonov, V. N.; Kadam, R. M.; Mandal, S. K.; Adhikari, R.; Das, A. K.; Nath, T. K.; Ganguli, N.; Dasgupta, I.; Das, G. P. *Phys. Rev. B: Condens. Matter Mater. Phys.* **2010**, *81*, 184421.
(43) Kwak, W.-J.; Lau, K. C.; Shin, C.-D.; Amine, K.; Curtiss, L. A.; Yang-Kook, S. *ACS Nano* **2015**, *4*, 4129.
(44) Cristol, S.; Paul, J. F.; Schovsbo, C.; Veilly, E.; Payen, E. *J. Catal.* **2006**, *239*, 145.
(45) Ren, X. D.; Zhu, J. Z.; Du, F. M.; Liu, J. J.; Zhang, W. Q. *J. Phys. Chem. C* **2014**, *118*, 22412.
(46) Ren, X.; Wang, B.; Zhu, J.; Liu, J.; Zhang, W.; Wen, Z. *Phys. Chem. Chem. Phys.* **2015**, *17*, 14605.
(47) Radin, M. D.; Rodriguez, J. F.; Tian, F.; Siegel, D. J. *J. Am. Chem. Soc.* **2012**, *134*, 1093.
(48) Chase, M. W. *NIST-JANAF Thermochemical Tables*, 4th ed; American Institute of Physics: Melville, NY, 1998.
(49) Mo, Y. F.; Ong, S. P.; Ceder, G. *Phys. Rev. B: Condens. Matter Mater. Phys.* **2011**, *84*, 205446.
(50) Zhong, L.; Mitchell, R. R.; Liu, Y.; Gallant, B. M.; Thompson, C. V.; Huang, J. Y.; Mao, S. X.; Shao-Horn, Y. *Nano Lett.* **2013**, *13*, 2209.
(51) Mitchell, R. R.; Gallant, B. M.; Shao-Horn, Y.; Thompson, C. V. *J. Phys. Chem. Lett.* **2013**, *4*, 1060.
(52) Tompsett, D. A.; Islam, M. S. *Chem. Mater.* **2013**, *25*, 2515.
(53) Lee, S. W.; Carlton, C.; Risch, M.; Surendranath, Y.; Chen, S.; Furutsuki, S.; Yamada, A.; Nocera, D. G.; Shao-Horn, Y. *J. Am. Chem. Soc.* **2012**, *134*, 16959.
(54) Vojvodic, A.; Norskov, J. K. *Science* **2011**, *334*, 1355.
(55) Esswein, A. J.; McMurdo, M. J.; Ross, P. N.; Bell, A. T.; Tilley, T. D. *J. Phys. Chem. C* **2009**, *113*, 15068.
(56) Rossmeisl, J.; Qu, Z. W.; Zhu, H.; Kroes, G. J.; Nørskov, J. K. *J. Electroanal. Chem.* **2007**, *607*, 83.

DOI: 10.1021/jacs.5b07792
J. Am. Chem. Soc. 2015, 137, 13572−13579